Electronic properties of $FeCl_3$-intercalated single-wall carbon nanotubes

X. Liu, T. Pichler, M. Knupfer, and J. Fink
Leibniz-Institut für Festkörper- und Werkstoffforschung Dresden, D-01069 Dresden, Germany

H. Kataura
Nanotechnology Research Institute, National Institute of Advanced Industrial Science and Technology (AIST) 1-1-1 Higashi, Tsukuba, Ibaraki 305-8562, Japan

(Received 17 May 2004; published 8 November 2004)

The electronic properties of $FeCl_3$ intercalated single-wall carbon nanotubes were investigated using high-resolution electron energy-loss spectroscopy in transmission and optical spectroscopy. The lowering of the nanotube Fermi level is directly measured via electronic excitations from C 1*s* to empty carbon 2*p* states derived from the doping. The charge induced disappearance of the optically allowed transitions is demonstrated by the evolution of the optical absorption spectrum. In the loss function the appearance of a new feature can be assigned to plasmon excitations. The optical properties of $FeCl_3$ intercalated nanotubes are comparable with those of fully potassium doped nanotubes. Upon annealing, the intercalant can be removed reversibly.

DOI: 10.1103/PhysRevB.70.205405 PACS number(s): 73.22.−f, 78.67.Ch

I. INTRODUCTION

Single-wall carbon nanotubes (SWCNT's) constitute a new class of materials, they exhibit semiconducting as well as metallic behavior depending on their geometrical structure defined by their chirality.[1–4] Owing to their unique structural and electronic properties, nanotubes could cover the full range of properties important for technology. Nanoscale applications of compound materials in electronic devices, nanosensors or as gas storage material are intensively explored. All these potential applications of SWCNT's depend upon the ability to modify their intrinsic properties by manipulating their structure and/or their electronic properties. A promising route for modification of SWCNT's is to add electron acceptors or donors in a controlled manner, so-called intercalation/doping.[5–10] An alternative would be chemical modification via substitution of carbon atoms by e.g., boron [11] or the addition of organic side-groups (so-called functionalization),[12,13] which leads to SWCNT's soluble in organic solvents and water, and could eventually lead to the control of the nanotubes upon external stimuli.

From optical absorption studies of doped SWCNT's compounds,[5,6] the disappearance of several absorption peaks upon doping has been assigned to electron depletion from or filling of specific bands in the semiconducting or metallic tubes, and the results demonstrate that nanotubes support amphoteric doping behavior. Furthermore, doping of SWCNT's by exposing them to potassium or bromine vapors has been shown to decrease their resistivity by more than one order of magnitude.[7] This means that it is possible to tune the Fermi level of SWCNT's, and thus to modify their electronic structure by changing their electronic density of states.[10] However, physical quantities such as the exact position of the Fermi level, have only been indirectly estimated from experimental studies of intercalated systems.

In this contribution, we report direct measurements of the distribution of previously occupied carbon 2*p* states which are depopulated through the nanotubes' reaction with an acceptor intercalant, $FeCl_3$, using high-resolution electron energy-loss spectroscopy (EELS) in transmission and optical spectroscopy. Owing to the shift of the Fermi level into the valence band, the suppression of previously optically allowed transitions is clearly shown from the evolution of the optical spectrum with increased doping. The appearance of a new feature in the EELS spectrum can be assigned to plasmon excitations. The optical properties at full doping are comparable with those in the fully potassium doped nanotubes. Upon high temperature annealing in vacuum, the intercalant is removed and the doping behavior is almost completely reversible.

II. EXPERIMENT

SWCNT's used for our studies were produced by laser ablation and had a mean diameter of 1.37 nm.[14,15] Thin films with an effective thickness of about 100 nm were prepared by dropping an acetone suspension of SWCNT's onto KBr single crystals. After the KBr was dissolved in distilled water, the films were transferred to a standard 200 mesh platinum electron microscopy grid. Firstly, the SWCNT films on grids were heated up to 500 °C for several hours in ultrahigh vacuum (UHV) to remove the organic contaminations in the films. Doping was performed by a two-zone heat treatment in a quartz tube.[16] SWCNT films and $FeCl_3$ were sealed within a quartz tube at a pressure of 2×10^{-8} mbar. For intercalation, the nanotubes were held at 300 °C at one end of the quartz tube and $FeCl_3$ was evaporated from the opposite end by heating it to temperatures between 100 and 280 °C to control the doping levels. Applying 280 °C the highest doping level was reached. This is also revealed by saturation of all changes as discussed below. The optical absorption measurement were performed using a Bruker IFS88 system with a resolution of 2 cm^{-1}. The SWCNT films were kept in the quartz tube for the measurements. After that, the quartz tube was opened in a nitrogen atmosphere and the intercalated SWCNT films were transferred into the measurement chamber (base pressure 2×10^{-10} mbar) of the purpose-built

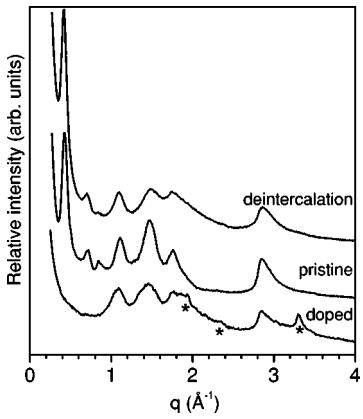

FIG. 1. The electron diffraction pattern of SWCNT's with $FeCl_3$ doping (bottom), the stars label the features arising with $FeCl_3$ intercalation. For comparison, the spectra of the pristine nanotube (middle) and the de-intercalated one (top) are also shown.

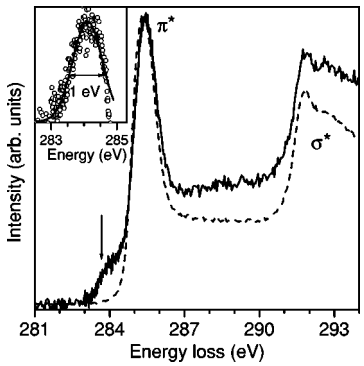

FIG. 2. C 1*s* core-level excitations of pristine (dashed line) and $FeCl_3$-doped SWCNT's (solid line). The arrow indicates the additional empty states due to doping. The inset shows the difference between the spectral weight of doped and pristine nanotubes after normalizing the two spectra at the $\pi^\star$ states (Ref. 28).

170 keV EELS spectrometer[17] with the energy and momentum resolution being 180 meV and 0.03 Å^{-1} for the low energy-loss function and electron diffraction, and 300 meV and 0.1 Å^{-1} for core-level measurements. All EELS measurements are carried out at room temperature. The deintercalation is achieved by heating the sample up to 500 °C in UHV.

III. RESULTS AND DISCUSSION

A. Electron diffraction

In laser ablated SWCNT's, the individual nanotubes can coalesce into long crystalline bundles, arranged in a hexagonal lattice by van der Waals forces.[18,19] In a bulk sample, there is a mixture of nanotubes with different diameters and lengths. From diffraction experiments, the intertube distance and the mean diameter of SWCNT's can be obtained.[20–22] When nanotubes are exposed to $FeCl_3$ gas, for an isolated SWCNT, binding sites of the intercalant are located at the external surface of the tube through physisorption or chemisorption, and presumably in the interior of the tube if its ends are open. In SWCNT bundles, it is considered that the intercalated species are located in the interstitial channels and the lattice expansion depends on the tube diameter and the dopant size.

Figure 1 depicts the electron diffraction pattern of the $FeCl_3$-doped SWCNT's as compared with the pristine and deintercalated ones. In the electron diffraction experiment, the diffraction pattern at lower momentum transfer q (less than 2 Å^{-1}) can be assigned to bundle diffraction, and that in the higher q region is ascribed to in-plane contributions of the graphene layers. From Fig. 1 it can be seen that the first bundle peak of $FeCl_3$ doped SWCNT's completely disappears due to strong lattice expansion and doping-induced disorder in the nanotube bundles; meanwhile, additional signals assigned to $FeCl_3$ appear in the spectrum, marked as stars. It is generally assumed that evaporated $FeCl_3$ enters the nanotube sample as $(FeCl_3)_2$ dimers[23,24] which are platelets with a lateral radius of about 6.1 Å and a vertical extension of about 1.5 Å. Due to the size of the dimers, bundles containing a lot of SWCNT's with diameters below about 1.2 nm cannot be intercalated. This is in complete agreement with Raman studies of $FeCl_3$ intercalated SWCNT's with a mean diameter of 1.07 nm and a broad diameter distribution.[23,24] After heating up to 500 °C, the nanotube bundle peaks are almost completely recovered (see top curve in Fig. 1), the slight difference to the pattern of pristine SWCNT's can be assigned to a larger disorder after the intercalation and deintercalation process. However, from the point of our structural analysis, $FeCl_3$ doping behavior is reversible.

B. Core-level excitations

Information on the electronic structure of intercalated SWCNT's can be extracted from the analysis of the core-level excitations at the C 1*s* excitation edge using EELS. Transitions from the localized core states to empty π orbitals are probed. For the pristine SWCNT's (see the dashed line in Fig. 2), the spectral features correspond to transitions into C 2*p*-related (unoccupied) $\pi^\star$ and $\sigma^\star$ electronic states. The former are characterized by a nearly symmetric peak centered at around 285.4 eV and the latter start at 292 eV, which are similar energies as observed for the analogous excitations in graphite.[25] In addition, the SWCNT spectrum closely resembles an average of the in-plane and out-of-plane graphite spectra due to the curvature effect and polycrystallinity.[26] Due to the effect of the C 1*s* core hole in the final state, both the $\pi^\star$ and $\sigma^\star$ onsets are dominated by spectral weight resulting from the influence of the core hole.[25,27] Therefore, no peaks related to singularities of the density of states of the different types of SWCNT's are observed.

Figure 2 shows the C 1*s* spectrum of $FeCl_3$-doped SWCNT's as compared to that of pristine SWCNT's. The $\pi^\star$ peak shows a similar shape as for the pristine nanotubes at an energy of 285.5 eV, accompanied by a new structure between 283 and 285 eV (as indicated by the arrow). Since $FeCl_3$ is an electron acceptor, in the intercalated SWCNT compound, charge is removed from the nanotube valence band creating new empty states which were occupied before intercalation. The C 1*s* excitation spectrum now includes

transitions into these empty π orbitals localized on the carbon atoms giving rise to the new structure shown in Fig. 2. Furthermore, there is a small shift of the $\pi^\star$ peak to higher energy, which is most likely due to an increase of the carbon 1*s* binding energy caused by the reduced net charge on the carbon atoms due to $FeCl_3$ doping.

Additional information about the charge transfer from the valence band of the SWCNT's to the $FeCl_3$ molecules can be derived from analyzing the spectral weight under the C 1*s* excitation edge. As mentioned above, transitions from the localized core states to empty π and σ orbitals are probed. Although one has to take into account strong excitonic effects, the additional spectral weight can be attributed to transitions into former valence band states which have been depopulated by the intercalation induced charge transfer. A detailed analysis of the transferred charge can be extracted from the difference in the spectral weight of the pristine and the doped SWCNT's. In analogy to $FeCl_3$-intercalated graphite,[16] the onset of the new charge transfer induced peak (CT-peak) can be taken as a measure of how much the Fermi level has been lowered upon intercalation (see inset of Fig. 2). The resulting shift of the Fermi level is about 1.0 eV. This is consistent with the shift of the Fermi level derived from optical absorption measurements (see below). Furthermore, from the comparison between the intensity of the new CT-peak and the total spectral weight of the $\pi^\star$ states in the pristine SWCNT's a charge transfer of about $0.12e^-$ per carbon atom can be derived. This *p*-type doping is similar to *n*-type doped SWCNT's compounds, where the $\pi^\star$ intensity decreases by about 10% in potassium doped samples with $C/K \sim 8$.[29] Thus, we can conclude that with *n*- and *p*-type doping of SWCNT's one can reach the same doping level.

C. Valence band excitations

In a bulk sample, the SWCNT films contain nanotubes with different diameters and chiralities, e.g., semiconducting and metallic nanotubes, thus the experimental signal represents an average of their responses. Optical absorption spectra of the pristine films clearly reflect this average with broad absorption peaks.[14,15] The first two peaks around 0.7 and 1.2 eV correspond to the first two interband transitions between the van Hove singularities in the electronic density of states of semiconducting SWCNT's. The peak at around 1.8 eV results from transitions between the first set of singularities in the density of states of the metallic nanotubes. All these features are superimposed on the low energy tail of a broad absorption peak located at roughly 5 eV (assigned to π-$\pi^\star$ transitions). The depletion of electrons in the valence band of $FeCl_3$ doped nanotubes leads to a suppression of previously allowed optical transitions as the initial states become emptied, which is reflected in the optical absorption measurements.

Figure 3 shows the evolution of the optical absorption spectra with increasing $FeCl_3$ concentrations as compared with that of the pristine SWCNT's (top curve) in the energy range between 0.3 and 2.5 eV. With increasing $FeCl_3$ intercalation the optical spectra show an intensity decrease of the transitions related to the lowest interband transition of the semiconducting SWCNT's (E_{11}^S). Finally this E_{11}^S absorption peak disappears. Increasing the doping level further, the second (E_{22}^S) peak becomes weaker, until it also completely disappears. As a consequence of doping, eventually, all optical transitions representative of the undoped tubes disappear. In a simple rigid band consideration this corresponds to a shift of the Fermi energy of at least 1.0 eV, since for the metallic SWCNT's the absorption peak related to the first optically allowed transition E_{11}^M disappeared. After the disappearance of the optical transitions, one new peak appears in the absorption spectrum at an energy around 1.1 eV. The energy of this doping induced absorption feature increases with increasing doping. Thus, this peak cannot result from interband transitions as this would imply a constant excitation energy. Instead, this peak can be assigned to the response of collective excitations of the introduced holes by $FeCl_3$ doping. Hence, it is related to a charge carrier plasmon which is strongly damped and the actual plasmon energy as derived from the EELS data shown below is roughly at the high energy inflexion point (see the dashed arrow in Fig. 3).

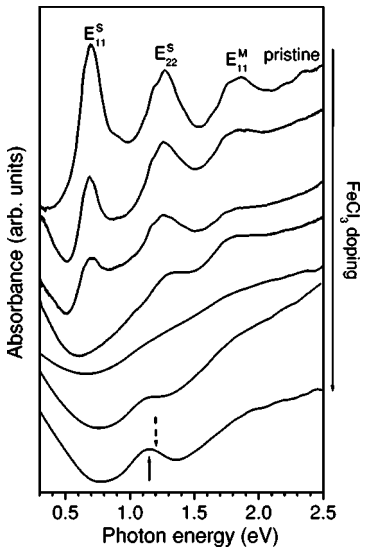

FIG. 3. The evolution of the optical absorption spectrum with increasing $FeCl_3$ doping. From top to bottom the doping level increases. The arrow in the bottom spectrum indicates the doping-induced optical peak. Dashed arrow points out the plasmon energy.

Next, we turn to a more detailed analysis of the charge carrier plasmon and the interband excitations by analyzing an EELS measurements. EELS in transmission measured using low momentum transfers probes the optical limit, thus the low-energy peaks in the loss function are due to collective excitations caused by optically allowed excitations.[30] The disappearance of structures in the EELS spectra can thus also be interpreted as the depletion or filling of electrons in specific bands. Features that arise during the intercalation process can be assigned to new, intercalation-induced excitations.[31,32]

Figure 4 shows the loss function of saturation $FeCl_3$-doped SWCNT's compared to those of pristine and deintercalated samples within the energy range of 0.2–60 eV at a momentum transfer $q = 0.15$ Å^{-1}. The wide peak at

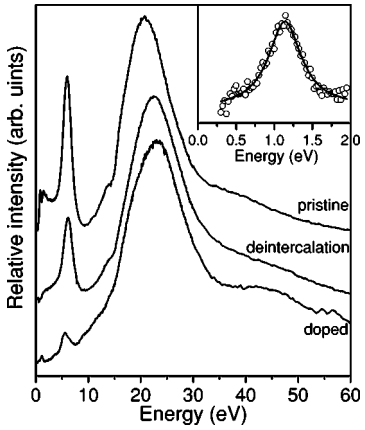

FIG. 4. Comparison of the loss function of fully $FeCl_3$-doped SWCNT's (bottom) with de-intercalated (middle) and pristine SWCNT's (top) at a momentum transfer $q=0.15$ Å^{-1}. The inset shows the fitting analysis (solid line) of the Drude plasmon in the loss function of the doped sample (open circle).

around 6 eV is the π plasmon related to π-$\pi^{\star}$ excitations in SWCNT's, the other broad peak at 23 eV represents the $\pi+\sigma$ plasmon resulting from the collective excitation of all valence electrons.[30] It can be clearly seen that in $FeCl_3$-doped SWCNT's the upshift of the $\pi+\sigma$ plasmonis about 2.6 eV and the downshift of π plasmon is about 0.5 eV. In addition, the intensity of the π plasmon strongly decreases upon doping. Fe 3*p* shallow core level excitations are observed at 54.5 and 56.6 eV. Focusing on the lower energy region below 3 eV, the peaks related to the above mentioned optically allowed interband transitions completely disappear, which is consistent with the optical data. An additional peak appears in this energy region which can be associated with the doping induced charge carrier (Drude) plasmon, similar to the alkali-metal doped nanotubes.[9,29] The most dramatic property of the new peak is a rapid loss of spectral weight with increasing momentum transfer up to 0.3 Å^{-1}, while this plasmon shows nearly no dispersion with increasing momentum.

In order to obtain further information on the electronic properties, the loss function of the fully $FeCl_3$ intercalated SWCNT's has been analyzed within the framework of a Drude-Lorentz model,[9,29] where the loss function of the intercalated SWCNT's can be assigned to three main features, a charge-carrier plasmon, one interband oscillator giving rise to the π plasmon, and another oscillator for the $\pi+\sigma$ plasmon. These are sufficient to explain the optical properties of the fully doped compounds (for details see Refs. 9 and 29). The impact of the higher-energy excitations on the Drude plasmon can be described by an effective screening with a background dielectric function ϵ_∞. This simulates the fact that the higher energy excitations screen the charge carrier plasmon which leads to a shift to lower energies as compared to its unscreened value. The fitting analysis yields the dielectric background $\epsilon_\infty=7$, the unscreened Drude plasmon $E_p=3.33$ eV, its damping $\gamma_0=0.52$ eV, and the optical conductivity at the zero frequency $\sigma_0=2868$ S/cm. The inset of Fig. 4 shows the results of the fitting procedure in the energy range of the charge carrier (Drude) plasmon. Compared to fully *n*-type (alkali metal) doped SWCNT compounds, the optical conductivity is very similar, which means that *n*-type and *p*-type doping can be carried out to the same level.

At last, by heating the doped sample up to 500 °C, the loss function of pristine SWCNT's can be recovered, as shown in Fig. 4. The Drude plasmon disappears, the previously optically allowed interband transitions appear, the intensity of the π plasmon is enhanced, and the $\pi+\sigma$ plasmon downshifted. Consequently, the intercalation process can be essentially reversed.[33]

IV. SUMMARY

In summary, studies of the structure, the unoccupied electronic states and of the optical properties of $FeCl_3$-intercalated SWCNT bundles using EELS in transmission and optical absorption have been presented. The intercalation modifies the bundle structure of SWCNT's. In $FeCl_3$-doped SWCNT's, the Fermi level shifts into the valence band as reflected by the disappearance of optical transitions and the additional pre-peak in the C 1*s* core-level excitations. At full doping a new, charge transfer induced peak is observed in both optical and EELS data. The EELS peak is assigned to the charge carrier plasmon which was analyzed within a Drude-Lorentz model. The results indicate that the optical properties of $FeCl_3$ (*p*-type) doped SWCNT's are comparable to those of the fully potassium (*n*-type) doped nanotubes. Upon heating, the structure and optical properties of pristine SWCNT's can be recovered.

ACKNOWLEDGMENTS

We acknowledge financial support from the DFG (PI440). Technical support by R. Hübel, K. Müller, and S. Leger is appreciated. H.K. thanks for support by the Industrial Technology Research Grant Program in '2003 from New Energy and Industrial Technology Development Organization (NEDO) of Japan.

[1] S. Iijima, Nature (London) **354**, 56 (1991).
[2] N. Hamada, S. Sawada, and A. Oshiyama, Phys. Rev. Lett. **68**, 1579 (1992).
[3] R. Saito, G. Dresselhaus, and M. S. Dresselhaus, *Physical Properties of Carbon Nanotubes* (Imperial College Press, London, 1998).
[4] J. W.G. Wildoer, L. C. Venema, A. G. Rinzler, R. E. Smalley, and C. Dekker, Nature (London) **391**, 59 (1998).
[5] R. Jacquemin, S. Kazaoui, D. Yu, A. Hassanien, N. Minami, H. Kataura, and Y. Achiba, Synth. Met. **115**, 283 (2000); S. Kazaoui, N. Minami, R. Jacquimin, H. Kataura, and Y. Achiba, Phys. Rev. B **60**, 13 339 (1999).

[6] T. Takenobu, T. Takano, M. Shiraishi, Y. Murakami, M. Ata, H. Kataura, Y. Achiba, and Y. Iwasa, Nat. Mater. **2**, 683 (2003).
[7] R. S. Lee, H. J. Kim, J. E. Fischer, A. Thess, and R. E. Smalley, Nature (London) **338**, 255 (1997).
[8] A. M. Rao, P. C. Eklund, S. Bandow, A. Thess, and R. E. Smalley, Nature (London) **388**, 257 (1997).
[9] T. Pichler, M. Sing, M. Knupfer, M. S. Golden, and J. Fink, Solid State Commun. **109**, 721 (1999).
[10] P. Petit, C. Mathis, C. Journet, and P. Bernier, Chem. Phys. Lett. **305**, 370 (1999).
[11] E. Borowiak-Palen, T. Pichler, A. Graff, R. J. Kalenczuk, M. Knupfer, and J. Fink, Carbon **42**, 1123 (2004).
[12] J. Chen, M. A. Hamon, H. Hu, Y. Chen, A. M. Rao, P. C. Eklund, and R. C. Haddon, Science **282**, 95 (1998).
[13] H. Kuzmany, A. Kukovecz, F. Simon, M. Holzweber, Ch. Kramberger, and T. Pichler, Synth. Met. **141**, 113 (2004).
[14] O. Jost, A. A. Gorbunov, W. Pompe, T. Pichler, R. Friedlein, M. Knupfer, M. Reibold, H.-D. Bauer, L. Dunsch, M. S. Golden, and J. Fink, Appl. Phys. Lett. **75**, 2217 (1999).
[15] H. Kataura, Y. Kumazawa, Y. Maniwa, I. Umezu, S. Suzuki, Y. Ohtsuka, and Y. Achiba, Synth. Met. **103**, 2555 (1999).
[16] E. J. Mele and J. J. Ritsko, Phys. Rev. Lett. **43**, 68 (1979).
[17] J. Fink, Adv. Electron. Electron Phys. **75**, 121 (1989).
[18] A. Thess, R. Lee, P. Nikolaev, H. Dai, P. Petit, J. Robert, C. H. Xu, Y. H. Lee, S. G. Kim, A. G. Rinzler, D. T. Colbert, G. E. Scuseria, D. Tomanek, J. E. Fischer, and R. E. Smalley, Science **273**, 483 (1996).
[19] A. G. Rinzler, J. Liu, H. Dai, C. B. Huffman, F. Rodriguez-Macias, P. J. Boul, A. H. Lu, D. Heymann, D. T. Colbert, R. S. Lee, J. E. Fischer, A. M. Rao, P. C. Eklund, and R. E. Smalley, Appl. Phys. A: Mater. Sci. Process. **67**, 29 (1998).
[20] D. Bernaerts, A. Zettl, N. G. Chopra, A. Thess, and R. E. Smalley, Solid State Commun. **105**, 145 (1998).
[21] H. Kuzmany, W. Plank, M. Hulman, Ch. Kramberger, A. Gruneis, T. Pichler, H. Peterlik, H. Kataura, and Y. Achiba, Eur. Phys. J. B **22**, 307 (2001).
[22] J. M. Cowley, P. Nikolaev, A. Thess, and R. E. Smalley, Chem. Phys. Lett. **265**, 379 (1997); L. Henrard, P. Bernier, C. Journet, and A. Loiseau, Synth. Met. **103**, 2533 (1999).
[23] A. Kukovecz, T. Pichler, R. Pfeiffer, and H. Kuzmany, Chem. Commun. (Cambridge) **16**, 1730 (2002).
[24] A. Kukovecz, T. Pichler, R. Pfeiffer, C. Kramberger, and H. Kuzmany, Phys. Chem. Chem. Phys. **5**, 582 (2003).
[25] P. A. Brühwiler, A. J. Maxwell, C. Puglia, A. Nilsson, S. Andersson, and N. Mårtensson, Phys. Rev. Lett. **74**, 614 (1995).
[26] M. Knupfer, Surf. Sci. Rep. **42**, 1 (2001).
[27] Y. Ma, P. Skytt, N. Wassdahl, P. Glans, J. Guo, and J. Nordgren, Phys. Rev. Lett. **71**, 3725 (1993).
[28] The higher background at higher energies and the corresponding enhancement of the σ^* edge is due to an increase of the multiple scattering resulting from the introduction of the $FeCl_3$ ions.
[29] X. Liu, T. Pichler, M. Knupfer, and J. Fink, Phys. Rev. B **67**, 125403 (2003).
[30] T. Pichler, M. Knupfer, M. S. Golden, J. Fink, A. G. Rinzler, and R. E. Smalley, Phys. Rev. Lett. **80**, 4729 (1998).
[31] J. J. Ritsko and M. J. Rice, Phys. Rev. Lett. **42**, 666 (1979).
[32] J. J. Ritsko and E. J. Mele, Phys. Rev. B **21**, 730 (1980).
[33] In the de-intercalated sample, the $\pi+\sigma$ plasmon is still at the higher energy compared with that of the pristine. One reason is the de-intercalation temperature (500 °C) is not high enough to achieve a complete recovery of the pristine sample but the trends show that the de-intercalation process is essentially reversible. Furthermore, in electron diffraction we observe a recovery of the original pattern concomitant with a higher background which might be due to reasons like a partial decomposition of the sample upon the heat treatment. This can also explain the incomplete recovery of the $\pi+\sigma$ plasmon in the low energy loss function.